applied sciences

MDPI

Article

Skin Absorbed Dose Coefficients for Human Legs from Beta Radiation as a Function of Height

Mohammad Yosofvand [1], Rabin Dhakal [1], Ali Nejat [2] and Hanna Moussa [3,*]

[1] Department of Mechanical Engineering, Texas Tech University, Lubbock, TX 79409, USA
[2] Department of Civil and Environmental Engineering, Texas Tech University, Lubbock, TX 79409, USA; ali.nejat@ttu.edu
[3] Department of Physics and Astronomy, Texas Tech University, Lubbock, TX 79409, USA
* Correspondence: hanna.moussa@ttu.edu

Abstract: External exposure to skin from beta-emitter radionuclides following severe reactor accidents or nuclear testing can result in beta burning and other health complications. The skin absorbed dose coefficient (SADC) measures the energy deposition into the skin during such accidents. The U.S. Environmental Protection Agency has published several reports to measure the possible energy deposition into the skin in such accidents. However, the most recent SADC published by Federal Guidance Report (FGR) 12 was computed only at one meter above the contaminated surface. Therefore, it was necessary to develop a model to estimate the absorbed dose coefficients for skin at different heights. In this manuscript, Geant4, a Monte Carlo simulator toolkit, was used to estimate the absorbed dose coefficients from electron sources located on the soil surface with energies ranging from 0.1 to 4 MeV. The energy deposited from primary electrons, secondary electrons, and photons in a 50 µm thick layer of epidermis tissue (Basal Cells Layer) located at a depth of 50 µm from the skin surface was estimated at several discrete heights of human leg phantom. More than 40% of the total energy deposited comes from secondary electrons and photons in energy sources of 0.1 and 0.2 MeV on average, but for higher energies, this percentage is less than 1%, which indicates primary electrons are the main source of the deposited energy in the skin. Furthermore, the results showed the energy deposited into skin closer to the ground was 50–100% higher than the previously estimated doses for 1 m above the ground. The results from Geant4 showed a great correlation (R^2 = 0.972) with the FGR 12 data at one meter height, and they were aligned with the published values from FGR 12, which validated the simulation results. Therefore, the calculated dose coefficients for different energy sources and different heights could be used in radiation protection measurements.

Keywords: skin absorbed dose coefficient; beta emission; radiation protection; Geant4

check for updates

Citation: Yosofvand, M.; Dhakal, R.; Nejat, A.; Moussa, H. Skin Absorbed Dose Coefficients for Human Legs from Beta Radiation as a Function of Height. *Appl. Sci.* **2024**, *14*, 7363. https://doi.org/10.3390/app14167363

Academic Editor: Paolo Branchini

Received: 26 May 2024
Revised: 1 August 2024
Accepted: 6 August 2024
Published: 21 August 2024

Copyright: © 2024 by the authors. Licensee MDPI, Basel, Switzerland. This article is an open access article distributed under the terms and conditions of the Creative Commons Attribution (CC BY) license (https://creativecommons.org/licenses/by/4.0/).

1. Introduction

At nuclear accident sites such as Chernobyl, workers at the plant were exposed to acute radiation. The emission cloud (fission products), the damaged reactor core, and other tools used in the plant were some of the sources of this acute exposure [1–3]. People within a 30 km radius were estimated to be exposed to high radiation doses. Workers who received less than 4 Gy during the accident were successfully treated. Also, those who were exposed to whole-body radiation between 4–6 Gy were moderately treated. However, about 30 patients exposed to more than 6 Gy radiation died due to skin burns or other consequences of acute exposure [4]. Approximately 115 patients were sent to Moscow to be treated there. Among them, 30% had skin burns covering 10–50% of their whole body, and roughly 11% had burns affecting 10–50% of their skin [5]. This damage to the workers' skin and bodies was due to the high exposure. Beta emission was one of the main sources of skin burns in the Chernobyl incident [6].

Reactor accidents or nuclear explosions can lead to fission products being deposited into the environment, contaminating water resources, air, and soil. During nuclear accidents, different particles such as beta particles, alpha particles, neutrons, and photons are emitted [7,8] from fission products.

Beta particles are electrons and positrons emitted from the nuclei of unstable atoms, and they have the same mass as electrons [9]. Beta particles can have either a negative or positive charge; a negatively charged beta particle is identical to an electron, while a positively charged one is identical to a positron [10]. Due to their small mass, high-energy beta particles can reach the speed of light [11]. They also lose their energy very fast when they interact with matter; consequently, their range in air or other materials is very limited. The damage that beta particles can cause to materials is less than that of other particles for the same deposited energy [12]. Beta with the negative charge "e^-" decays when a neutron "n" becomes a proton "p" and an antineutrino "$\overline{v}$" are emitted [13]:

$$n \rightarrow p + e^- + \overline{v} \quad (1)$$

A positron "e^+" (Beta particle with a positive charge) decays when a proton becomes a neutron and a neutrino "v" are emitted as [14]:

$$p \rightarrow n + e^+ + v \quad (2)$$

Beta particles are one of the main radiation products at nuclear accident sites that can cause severe skin burns as they can penetrate the outer layers of the skin [15–19]. Therefore, estimating the absorbed dose to human skin layers from beta emissions at contaminated incident sites is important. Beta decay from fission products has a spectrum energy ranging from a few keV to about 5 MeV [20,21]. Cross et al. studied the beta decay spectrum for about a hundred different radionuclides [22]. The energy spectrum range for the isotopes started from 0 to 4 MeV, and very few exceeded 4 MeV. In this manuscript, we limited the energy range for beta particles to 4 MeV and used the word electron to refer to beta particles unless it is mentioned otherwise.

The outer layer of the skin can act as a shield against very short-range radiation, such as alpha particles or beta particles with energy less than 60 keV, as beta particles below this energy range cannot penetrate the outer layer of the skin [23]. Beta emissions with higher energy particles than that threshold can damage the skin tissue; thus, several models have been developed to measure the energy deposited in human skin tissue due to beta emissions in health physics and biomedical studies. Faw et al. used a Monte Carlo simulation to calculate the absorbed dose deposited into human skin from different radionuclides that emitted beta particles [24]. VARSKIN 5 is a computer code that is widely used to calculate the absorbed dose to the skin [25]. Sherbini et al. compared and verified this program with the results from MCNP 5 calculations [26]. Amato et al. measured the accuracy of VARSKIN 5 with GAMOS, a Geant4-based health physics and medical physics simulator for beta sources. They calculated the absorbed dose at 70 μm depth of skin from the beta decay of 20 different radionuclides [27]. Similar Monte Carlo simulations were performed to estimate the absorbed dose from beta particles to health personnel in medical radiology centers [28]. Geant4 is a computer program based on C++ that simulates the interaction between different radioactive particles through matter, and it is widely used to estimate the absorbed dose estimations in Monte Carlo studies [29–32]. Recently, Frosio et al. used several simulation packages, including Geant4, to estimate the skin absorbed dose coefficient (SADC) [33]. Skin-absorbed dose coefficients are important values in radiation. In the event of a nuclear disaster, knowing these values for different radioactive emissions, including beta decay, would be essential for the safety of personnel and surrounding people.

Berger implemented Kocher and Berger's electron point kernels to calculate the absorbed dose from different beta emission sources [34]. He also included contributions from bremsstrahlung emissions based on the National Institute of Standards and Technology

(NIST) dataset. This dataset was used in Federal Guidance Report 12 to calculate the skin absorbed dose coefficient for human skin tissue located at 1 m above the soil contaminated with beta decay [35]. The U.S. Environmental Protection Agency has published several versions of these federal guidance reports over the past few decades to ensure the consistency of assessments of ionizing radiation [35,36]. This technical information provided in the most recent Federal Guidance Report, 12, is widely used for radiation protection in the U.S. to ensure the population's safety during unexpected incidents. This published data will be used in the current manuscript to ensure the accuracy of the results.

2. Materials and Methods

The Geant4 toolkit is widely used for health, medical physics, and biomedical applications [37–39]. In this manuscript, the Geant4 code is utilized to simulate the absorbed dose coefficient to the skin of a human leg from beta-emitter radionuclides located on a flat surface. The main objective of these simulations was to compute the deposited energy from beta decay to the basal layer of skin for the different range of energy sources. The computed energies were converted to absorbed doses, and the result at one meter above the ground was compared with the results from Federal Guidance Report 12. Furthermore, we calculated the energy deposited into the basal layer from secondary electrons and photons only and estimated the portion of this deposited energy from the whole absorbed energy.

To set up the environment, a full sphere was created. This sphere formed the boundary of the simulation universe, and it was divided into two separate regions. The bottom half of the sphere was filled with soil to create the ground area of the contaminated environment, and the top half was filled with air. The configuration of the universe is shown in Figure 1. The data from Federal Guidance Report 12 was used to determine the composition of the materials, including air and soil; the mass percentage of each element of the materials used in the simulations, as well as their density- are presented in Table 1. Furthermore, the air and soil distribution in the simulation environment was assumed to be homogeneous.

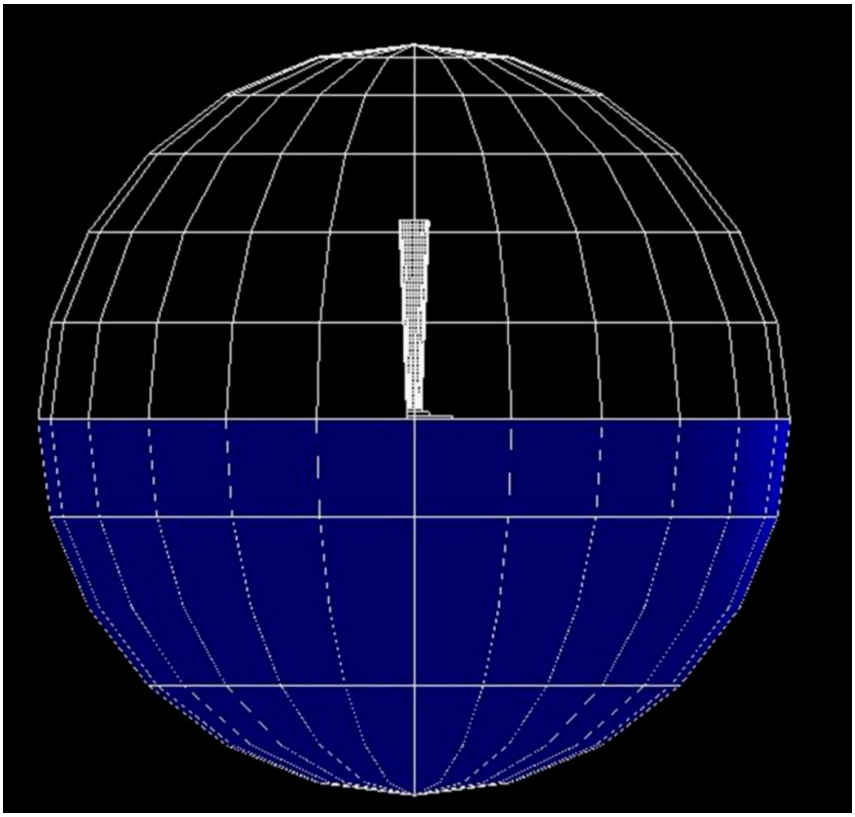


Figure 1. Simulation Universe Configuration. The blue hemisphere shows the soil and the above hemisphere is the air where the leg phantom is located.

Table 1. Table of Materials. The elemental composition by weight for each material and the density of each material used in the simulation are detailed.

Material	H	C	N	O	Na	Al	Si	P	S	Cl	K	Ca	Fe	Ar	Density (g/cm^3)
Tissue	10	20.4	4.2	64.5	0.2	0	0	0.1	0.2	0.3	0.1	0	0	0	1.09
Leather	9.08	19.14	4.8	67	0	0	0	0	0	0	0	0	0	0	1.15
Soil	2.1	1.6	0	57.7	0	5	27.1	0	0	0	1.3	4.1	1.1	0	1.60
Air	0.064	0.014	75.4	23.2	0	0	0	0	0	0	0	0	0	1.3	0.0012

The beta emission source was considered a cylindrical volume source set to correspond with the surface of the soil, with a depth of 1 μm, and the radius of the cylindrical source was set equal to the continuous slowing down approximation (CSDA) range of the electron particles in the air. The CSDA range is the average distance charged particles can travel through a medium [40]. The interaction between charged particles and atoms in the surrounding universe causes energy loss from the particles. The loss rate of the charged particle's kinetic energy equals the total stopping power. Thus, the CSDA range is calculated by the integral of the total stopping power for the particles in each medium with respect to the kinetic energy of the charged particle [41].

$$R(T) = \int_0^T \left(-\frac{dE}{dx}\right)^{-1} dE \tag{3}$$

R(T) is the range of a particle with kinetic energy (T) [42]. The unit for the range, R(T), is g·cm^{-2}. The range formula for beta particles with a kinetic energy of $0.01 \leq T \leq 2.5$ MeV is reduced to:

$$R(T) = 0.412 \times T^{(1.27-0.0954\times \ln(T))} \tag{4}$$

And for the kinetic energy of $T > 2.5$ MeV:

$$R(T) = 0.530 \times T - 0.106 \tag{5}$$

After calculating the range, R(T), for the desired electron energy, the CSDA was calculated by dividing it by the medium density:

$$CSDA = \frac{R(T)}{\rho} \tag{6}$$

where ρ is considered to be the density of air in this manuscript.

The beta decay source is assumed to be monoenergetic, emitting uniform and isotropic beta particles with a negative charge (electrons) in all directions (4π). The energy range for electrons varied from 0.1 MeV to 4 MeV, and different simulated values for the source are presented in Table 2. The source particles (electrons) were distributed uniformly in the cylindrical source. During each simulation, one energy range was assigned to the source; for example, the energy of the source was set to 0.1 MeV for all electrons.

Table 2. Source energies and corresponding CSDA ranges.

Energy (MeV)	CSDA Range (cm)	Energy (MeV)	CSDA Range (cm)
0.1	13.5	1.5	660
0.2	42	2.0	910
0.4	121	2.5	1150
0.8	310	3.0	1380
1.0	410	4.0	1840

The cylindrical source was placed at 1 μm depth in the soil, and its radius was set equal to the CSDA range of each electron's energy, as shown in Table 2. These CSDA ranges for electrons in the air are equal to those from the ESTAR program [43]. If the CSDA range for a given energy source was less than about 155 cm, which is slightly higher than the length of the leg, the radius of the cylindrical source was set to the CSDA range to save on simulation time because the electrons out of this range would not reach the leg. For energies equal to or higher than 0.8 MeV, the source radius and the simulation universe's radius were set to the corresponding CSDA range.

The target, the human leg skin, consists of different layers: the outermost layer of the skin is the Epidermis, the Dermis layer is placed underneath it, and the innermost layer of the skin is the Hypodermis. Each of these layers has different depths, which might vary based on the classification. Under the Hypodermis are the muscle layers [44]. The Epidermis layer is placed at the skin's surface, and there are no blood vessels in this layer; it is most crucial in body protection since it separates the body from the outside environment and protects it from external exposures, including low-energy beta particles [45].

The epidermis layer consists of five different layers, which function together to keep the skin surface healthy and repair it constantly. The innermost layer of the Epidermis is the Basal layer. It is placed right above the dermis layer; the basal layer is an active layer of skin that helps repair the outer sublayers of the Epidermis by constantly producing skin cells and replacing the damaged or older skin cells with new ones [46].

The basal cells are considered at the highest radiogenic risk when exposed to radiation due to their important role in repairing the skin. Therefore, in radiation protection, it is vital to calculate the absorbed dose to the basal layer of the Epidermis. The absorbed dose to the basal layer has been the main research topic of several studies due to radioactive or non-radioactive exposures to the skin [47,48]. Shih et al. studied the effects of ultra-violate radiation due to sunburns on the basal layer of the skin [49]. Eatough et al. studied the delivered dose to the basal layer of skin under alpha radiation exposure.

Moreover, basal cell carcinoma is the most common type of skin cancer in the U.S.; ionizing radiation exposure to the skin's basal cells can significantly increase the risk of basal cell carcinoma. Watt et al. showed that exposure of the basal cell layer to more than 1 Gy increased the risk of cancer [50]. Consequently, studying exposure to the basal layer is very important for radiation protection.

The thickness of the epidermis layer varies in different parts of the body. Moreover, the basal layer has an undulating nature, and the thickness is not the same in all parts. The International Commission on Radiological Protection (ICRP), in report 116, has recommended a thickness of 50 microns for the basal layer. They also recommended considering the start of the basal layer at a depth of 50 microns from the surface of the skin [51]. This modeling assumes that most basal cells are placed within 25 percent of the mean epidermal thickness at any desired area of the skin [52]. The mean values of epidermal thickness for different parts of the body were compared by Whitton et al. They showed that the basal layer of skin in the human leg starts at a depth of 40 μm from the skin surface to the depth of 93 μm, which is close to the recommended estimation from ICRP report 116 in terms of both placement and thickness [53]. Furthermore, ICRP Report 116 has suggested that basal cells should not be represented using reference voxel geometries when modeling the phantom for simulations.

The phantom of the human leg in the Geant4 Monte Carlo Simulation was modeled as 50 different truncated cones made of soft human tissue, as shown in Figure 2. The percentage of elements and the density of the skin tissue are considered to be the same as the soft tissue; they are presented in Table 1.

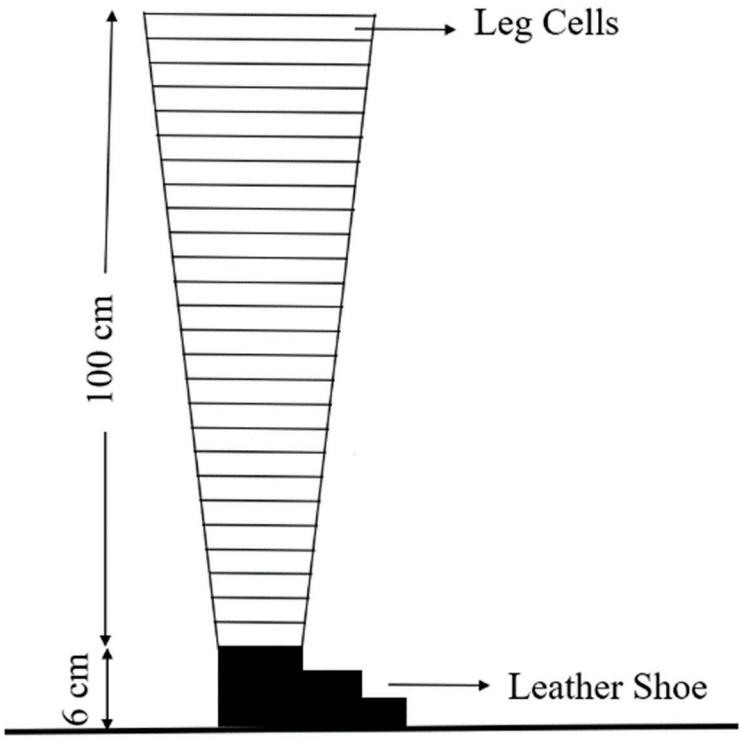


Figure 2. Leg phantom model.

In the modeling, the foot is modeled by three different cuboids stacking over each other, and it is assumed that the foot is covered by a leather shoe that is 6 cm in height in total. Table 1 shows the elemental composition of the materials. The phantom leg starts from 6 cm above the ground until 106 cm. The segmented cells are made of three upside-down, truncated cones inside each other and are 2 cm high. The innermost truncated cones represent the mixture of bones and muscles; they are also assumed to be made from soft tissue; the central truncated cone represents the basal cell layer (50 μm); and the outer truncated cone represents the surface layer (the dead layer cell of the skin), which is also considered 50 μm thick. Both the basal and the dead cell layers (the epidermis layer) are made from soft tissue; the basal layers (middle truncated cones) are considered to be detectors in the Geant4 simulations, and the absorbed dose to these parts of the cell is measured (Figure 3). The bottom radius, r, of the n-th truncated cones is calculated as follows:

$$r_{(\mathrm{cm})} = 4 + 0.08 \times (n - 1) \tag{7}$$

In this calculation, each cone's bottom radius equals the top radius of the underneath cone cell.

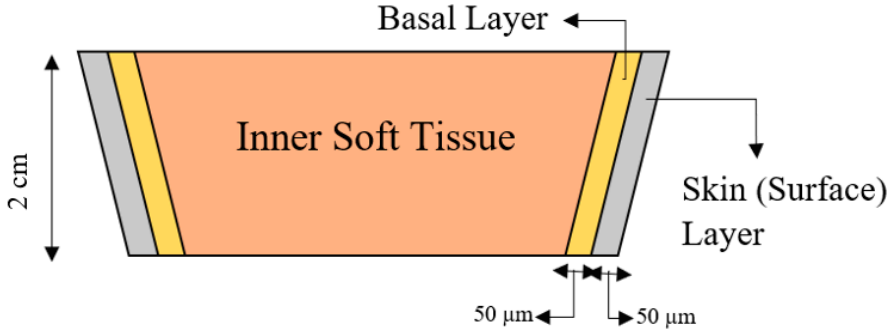


Figure 3. Cell layers for each truncated cone.

The negatively charged beta particles (primary electrons), secondary electrons, and generated photos were tracked during the simulation. The number of particles that hit the basal cell layer, as well as the deposited energy from these particles, were tallied and calculated using the "G4SDManager" class. For this purpose, a sensitive detector from this class was assigned to the basal layer in the leg phantom. Furthermore, the particles were eliminated if they hit the sphere border (Figure 1). The default physics simulator in Geant4 for intermediate energy particles (G4EmStandardPhysics) was acquired since the maximum beta particle was set to 4 MeV. This physics list processes ionization, bremsstrahlung, multiple scattering, the photoelectric effect, Compton scattering, and pair production. The physics parameters were set to the default values in the Geant4 simulation.

GENT4 version 10-04-patch-02 with multi-threading was used to obtain the results. The simulation time for the total of 2×10^9 iterations in Geant4 was very high, especially for the energy sources with more than 2.5 MeV. However, using the multi-threaded simulations in Geant4 further reduced the time of simulations while increasing the required processors and memory to perform the task. Using the C++ libraries makes Geant4 a fast toolkit in terms of using the multi-thread CPUs as well as the assigned memory, which helped in the simulations for this paper. To perform the simulations, two cluster nodes with 72 CPU cores (Intel Xeon E5-2695 v4) and 48 GB of RAM were used. The simulation time varied between 2 h for 0.1 MeV and 2.5 days for the 4.0 energy source. When the simulation ended for each energy source, the results from each thread were combined in Geant4, and the final deposited energy was calculated.

3. Results and Discussion

The skin absorbed dose coefficient (SADC) for different energy sources is calculated using Geant4 simulations for different heights of the leg; the total SADC and the SADC from primary electrons are compared to the SADC obtained from secondary electrons and photons. For each energy source, 2 billion beta particles were generated randomly from the cylindrical electron source at the top of the soil. The number of particles entering each detector as well as the deposited energy in keV were calculated. The mass for the basal layer was calculated using its volume and density.

The absorbed dose delivered to the basal layer was calculated by dividing the deposited energy by its mass, and then the absorbed dose per particle was calculated for each cell by dividing the absorbed dose by the total number of events generated. Finally, the SADC for each basal layer was calculated by multiplying the absorbed dose per particle by the source area, as follows:

$$SADC = \frac{E \times A}{M \times p} \tag{8}$$

where SADC is in $\mu G_y \cdot m^2$ per particle, E is the deposited energy in keV, M is the mass of the basal layer in kg, A is the area of the source in m^2, and p is the total number of generated particles. Similar calculations are conducted to calculate the SADC from secondary electrons and generated photons during the simulations.

The absorbed dose coefficient comparison between the total absorbed dose and the dose from primary electrons (electron only) for different heights of the leg is depicted for energy sources 0.1 MeV and 0.2 MeV in Figures 4 and 5, respectively. For the sources with low energies (0.1 and 0.2 MeV), primary electrons deliver a very low absorbed dose to basal cells, especially for the cells with heights greater than the CSDA range. The simulation results in Geant4 showed that for higher energies, more than 99% of the deposited energy in leg cells comes from the tracked primary electrons originating directly from the ground beta source. The absorbed dose coefficient for energy sources of 0.4, 0.8, and 1.0 MeV is shown in Figure 6. The total skin absorbed dose for energy sources of 1.5, 2.0, and 2.5 MeV, as well as the total skin absorbed dose for 3.0 and 4.0 MeV energy sources, are displayed in Figures 7 and 8, respectively.

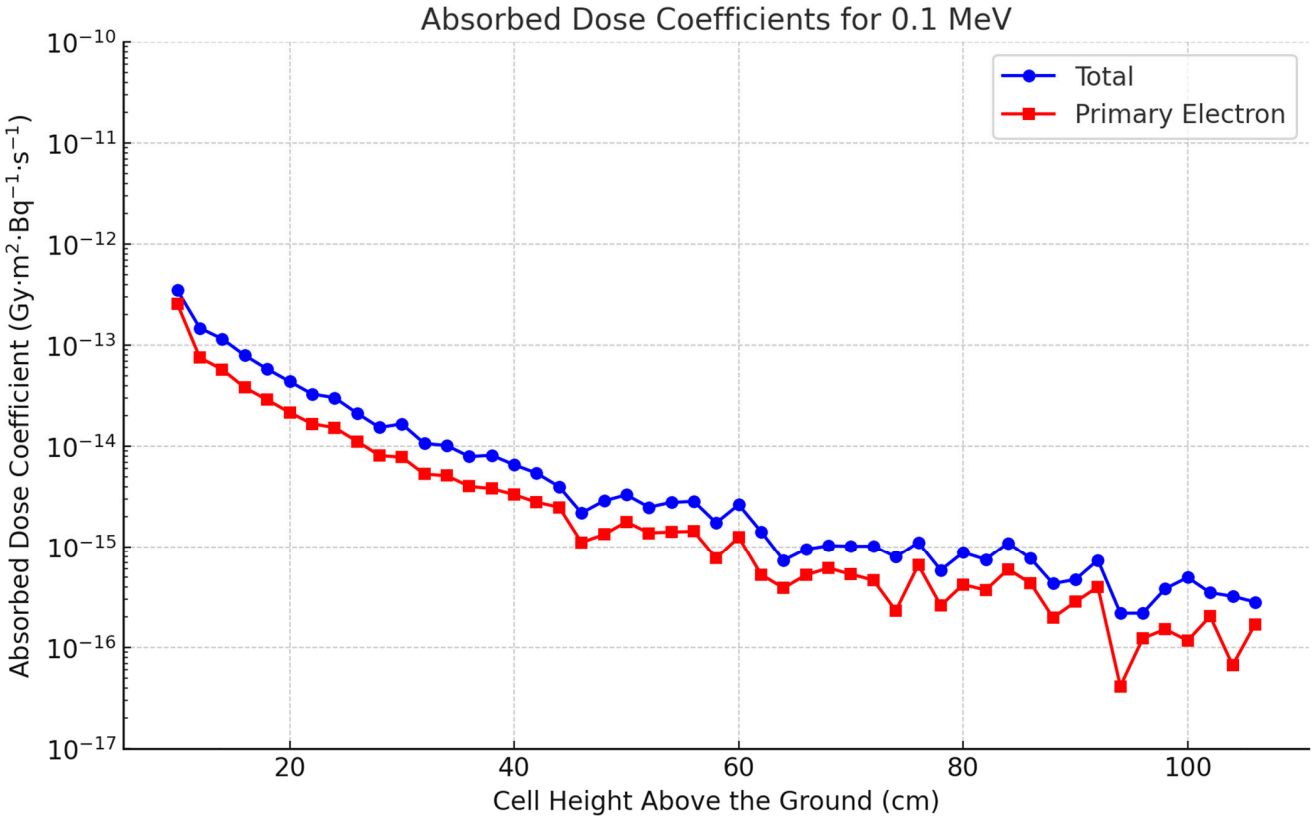


Figure 4. Skin absorbed dose coefficient for 0.1 MeV source for electrons only and total deposited energy.

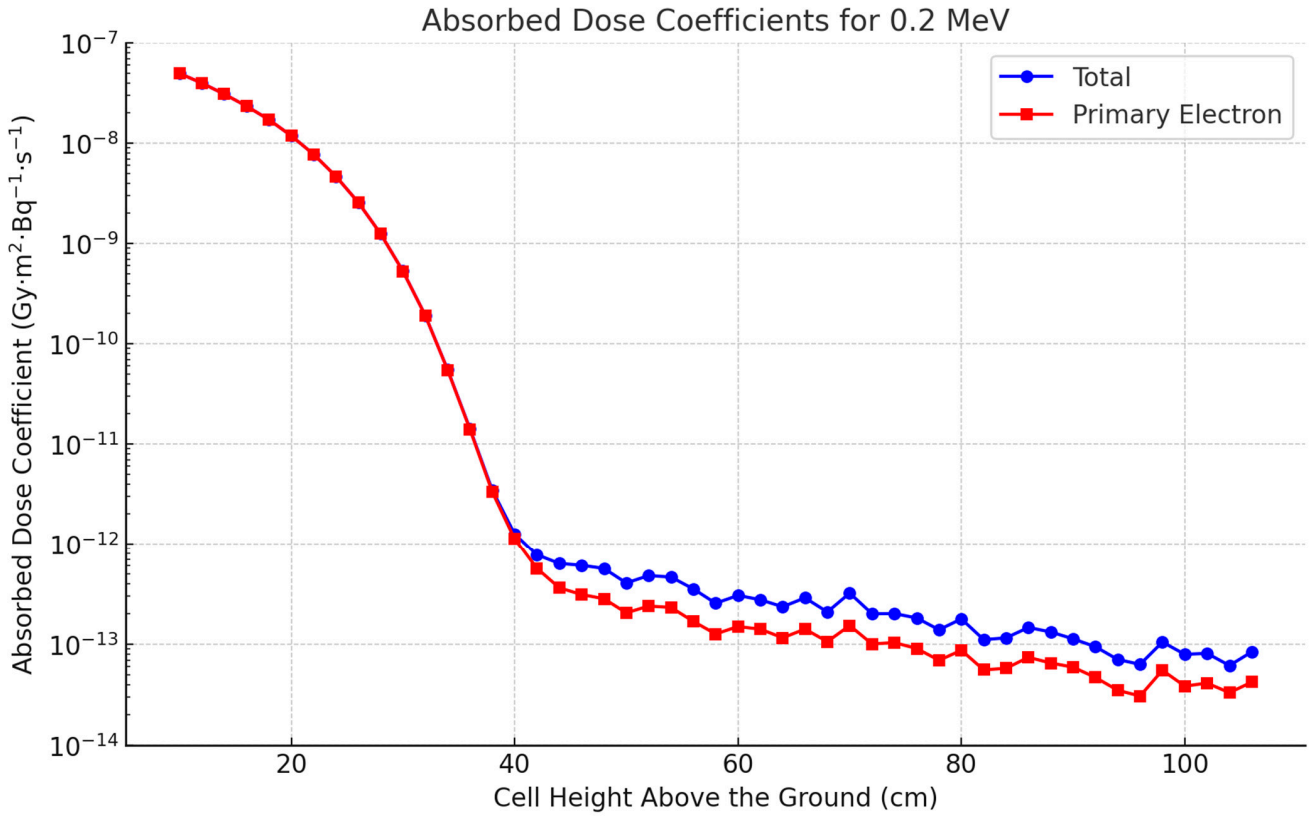


Figure 5. Skin absorbed dose coefficient for 0.2 MeV source for electrons only and total deposited energy.

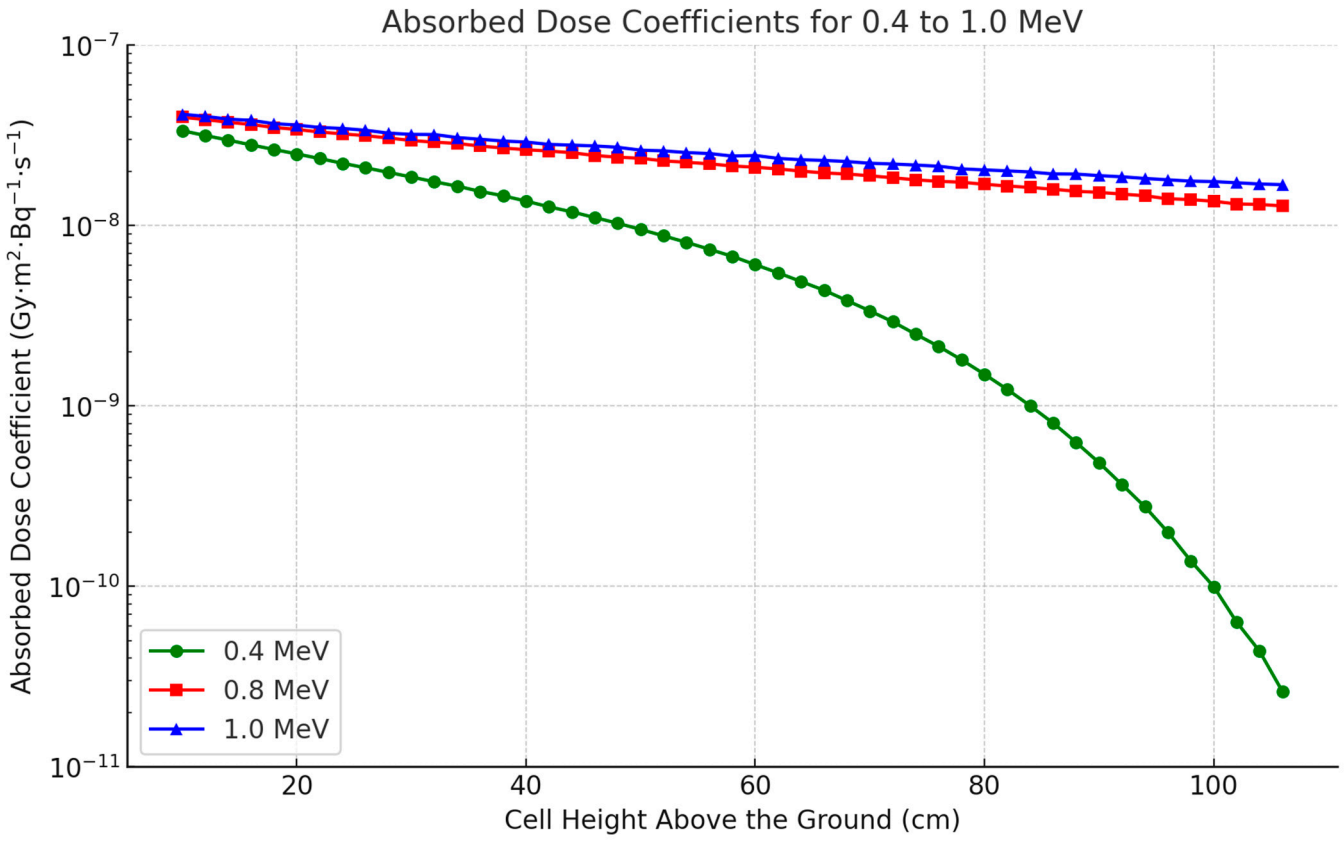


Figure 6. Total skin absorbed dose coefficient for 0.4, 0.8, and 1.0 MeV.

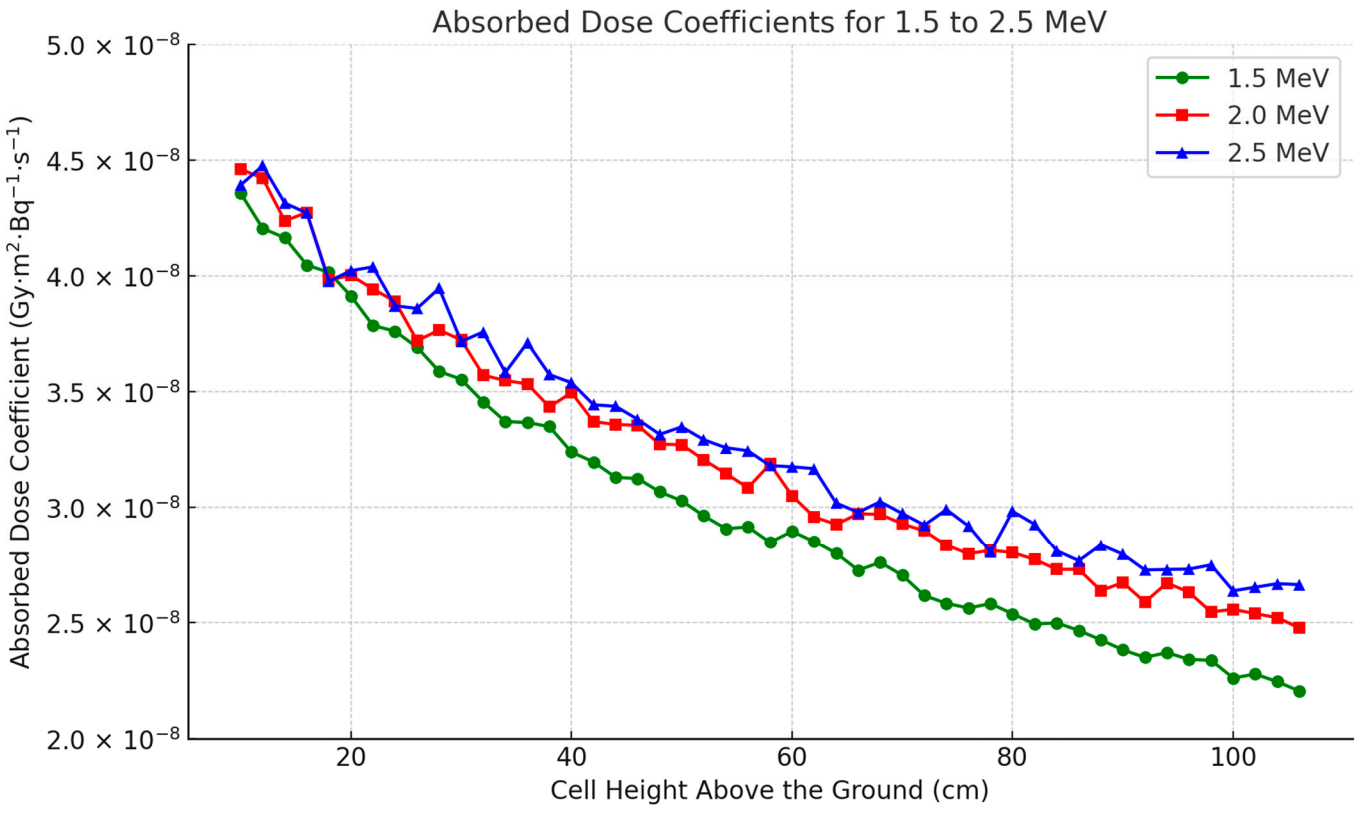


Figure 7. Total skin absorbed dose coefficient for 1.5, 2.0, and 2.5 MeV.

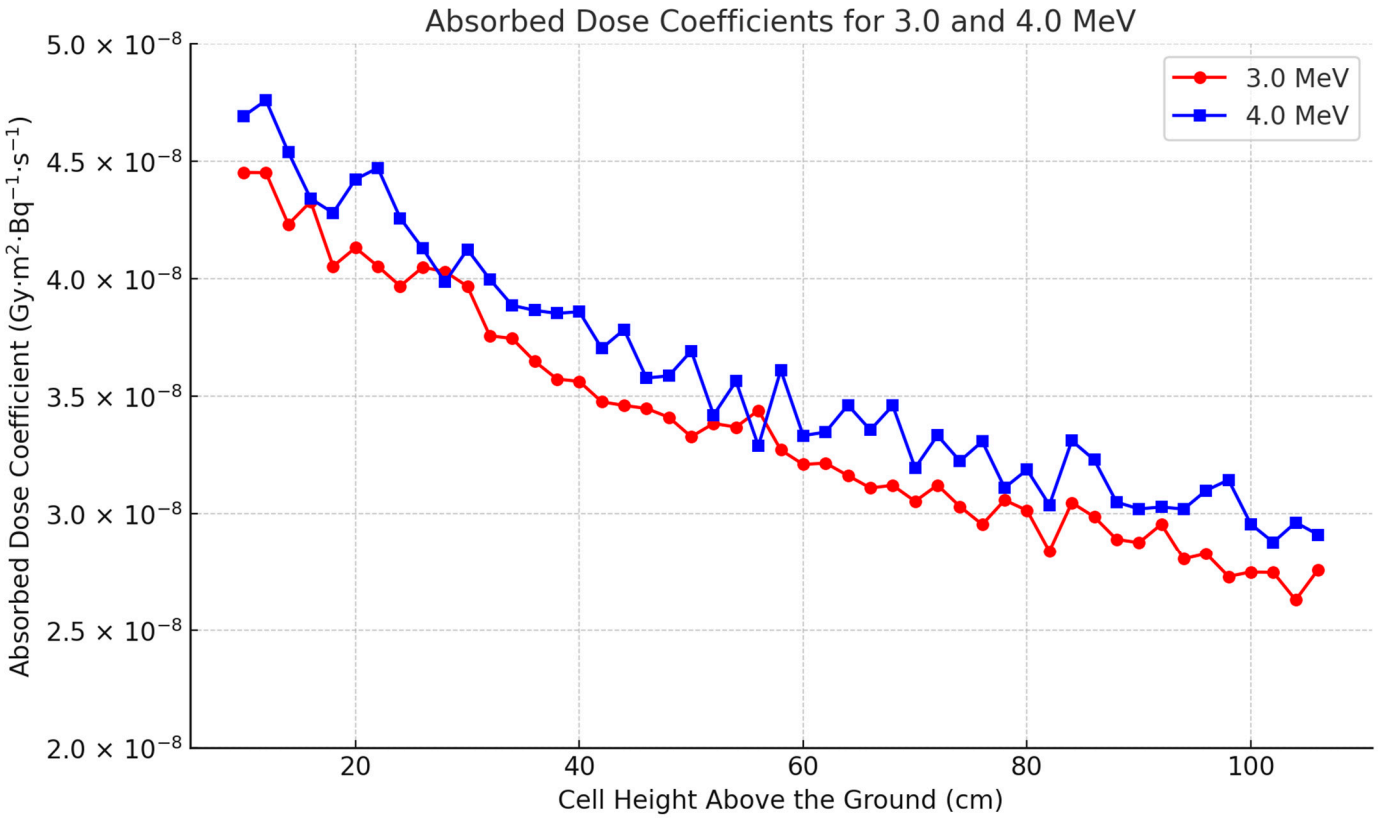


Figure 8. Total skin absorbed dose coefficient for 3.0 and 4.0 MeV.

For sources with lower energies (0.1 and 0.2 MeV), the share of generated photons and electrons in the deposited energy in the human leg cells was much higher. The share of secondary electrons and generated photons in the deposited energy in cells with a higher height than 10 cm (after the third cell) for the 0.1 MeV source jumped from 1% to more than 40% of the total deposited energy. The percentage of the absorbed dose from photons in the total deposited energy in the phantom leg is depicted in Figure 9. For the electron source with 0.1 MeV, when the height of cells exceeds the CDSA range (13.5 cm), a sharp increase in the percentage share of photons happens. Expectedly, the increase in the percentage share of photons for 0.2 MeV occurs for higher cells, as the CDSA range for 0.2 MeV is about 42 cm. For the source with 0.4 MeV, only the very top cell of the phantom leg has considerable deposited energy from photons. For the other energy sources, photons and secondary electrons make up less than 1% of the total deposited energy into the leg. Since it is expected from the physics of the problem to see this pattern in the deposited energies for different energy sources, this graph validates the simulation results.

Different factors could affect the results from the Geant4 simulations for the human leg. One major factor is the selection of the cross-section libraries from the Geant4 simulator. To avoid a large difference in the results, we conducted different simulations with different cross-section libraries; the differences in the results from different cross-section libraries were negligible. The important point during the simulations was using the same cross-section library for all energy sources. Another important factor that could play a significant role in the differences in the results is the pseudo-random number generator seeds in Geant4. Even when one simulator toolkit such as Geant4 is used, results can be different if the seeds are different [54]. To avoid that, we considered the number of events to be high enough; thus, the results would be statistically significant. Also, the same pseudo-random number generator seeds were used for all energy ranges studied in this paper. Furthermore, the numerical approximations in built-in physics functions that simulate the interaction,

the passage, and the generated secondary electrons or photons contribute to the variation in the results.

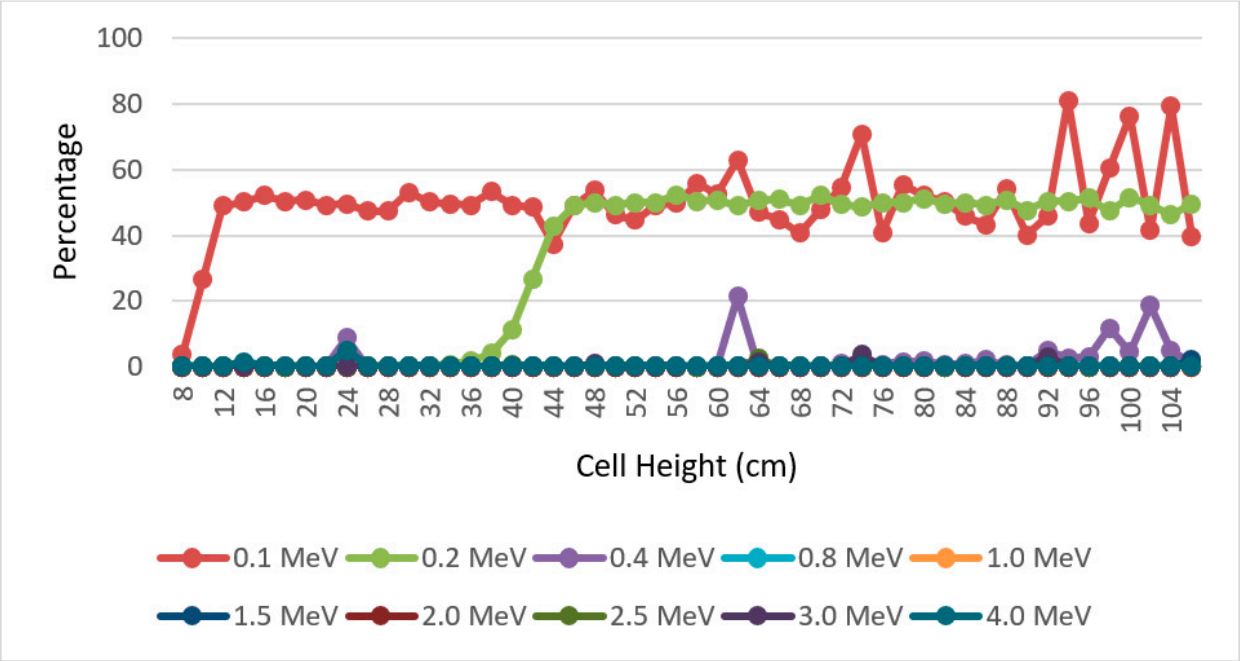


Figure 9. Secondary electrons and generated photons share from the deposited energy in the phantom legs. The percentages for energy sources from 0.4 MeV to 4.0 MeV overlapping as they are close to zero.

To further validate the results and expand the current data used in health physics and protection guidelines, the SADC from the simulations was compared with the results from the Federal Guidance Report (FGR) 12. FGR 12 calculated the skin dose coefficients for different source energies for the 1.00 m height above the contaminated area with beta particles. The comparison graph for the SADC for phantom cells at a height of 100 cm is plotted for Geant4 and the published values from FGR 12 (Figure 10). The minimum energy with available FGR 12 data were 0.4 MeV. For sources with low energy, the difference between the FGR 12 data and the calculated data from Geant4 is larger than the sources with higher energies; even though for lower energies, the difference is still acceptable. It can be observed from Figure 10 that for the sources with energies > 1.0 MeV, the difference between the calculated data and the published data from FGR 12 is negligible. Comparing the Geant4 data with the FGR 12 data for 1 m height, the R^2 value is 0.972 and the correlation coefficient is 0.986.

The calculated value for each cell in the leg phantom using the Geant4 simulations for different energy sources for both total deposited energy and the energy deposited from the primary electrons is provided in Table A1 in Appendix A at the end of the manuscript.

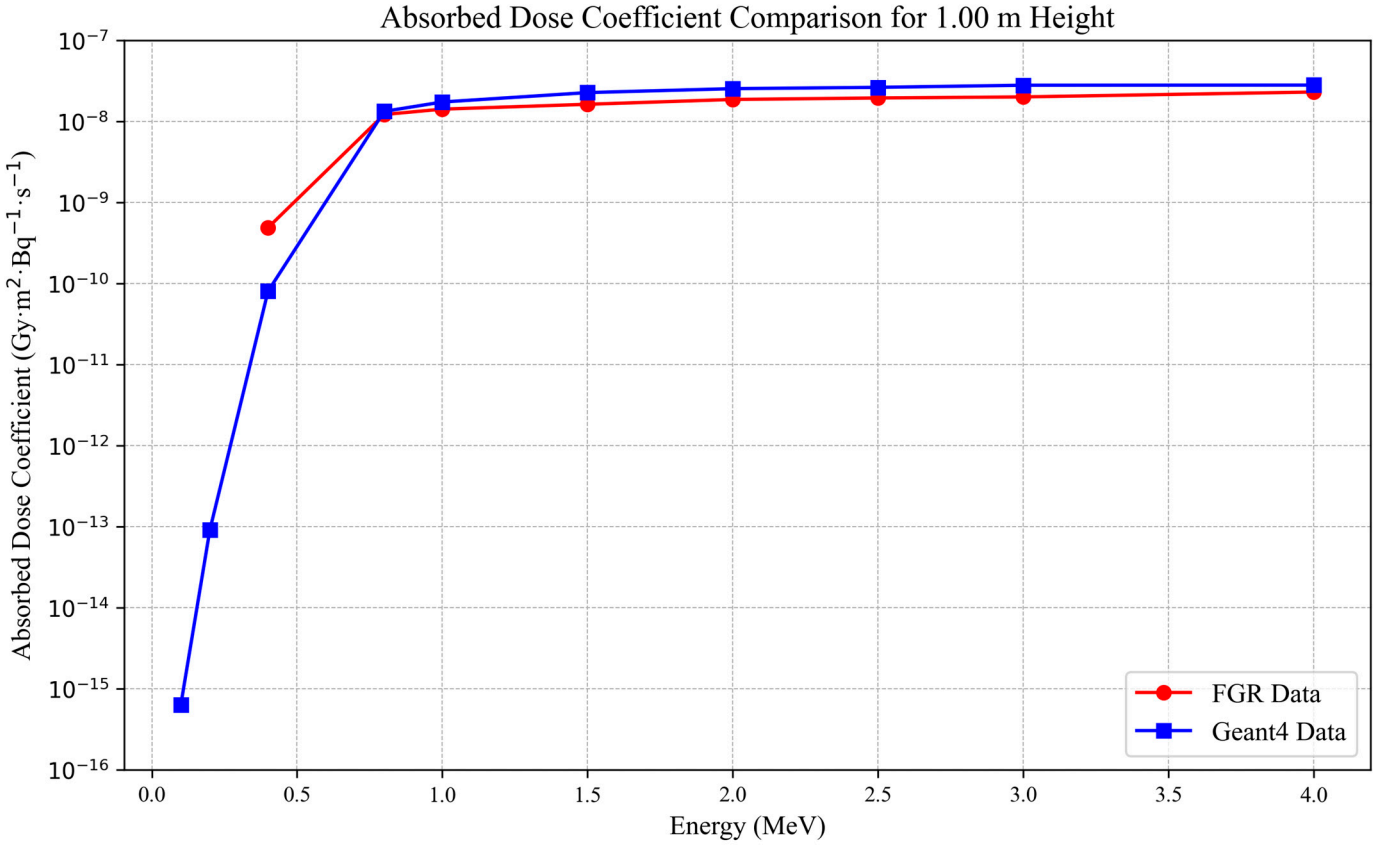


Figure 10. Skin absorbed dose comparison between FGR and Geant4.

4. Conclusions

Beta particles in accident sites are known to be one of the main contributors to skin burns and other health issues for personnel. In this paper, we concluded that it is necessary to expand the previous calculations for contaminated soil with beta particle decay for skin-absorbed doses to other heights above the ground. The energy deposited to the leg dosimeter near the ground from the beta decay is much higher than the deposited energy to the leg at 100 cm height. Thus, the actual absorbed dose by the skin can be higher than using the previous calculations, which makes it necessary to consider these findings in radiation protection measurements.

Furthermore, the comparison of the deposited energy between primary electrons and secondary electrons and the generated photons showed the primary electrons make almost all the deposited energy in the phantom cells (>99%) for energy sources greater than 0.4 MeV. However, for lower energy sources, the secondary electrons and photons made up most of the energy deposited in the phantom cells. This validated the simulation results. To further evaluate the results, statistical analysis was conducted, which proved the statistical significance of the results from this paper. The results from the Geant4 at 1 m height were compared with the SADC published by FGR 12, and the results were matched perfectly well with a significant *p*-value. Thus, we concluded that the results obtained from Geant4 are valid.

Since there is not much experimental data available, the results of this paper can be used in radiation protection measurements. It provides an excellent dataset for an unfortunate nuclear accident to help the power plant staff and the civilians around the contaminated area, as it is an expansion of the FGR 12 report, which only contains the skin-absorbed dose data for the height of 1 m. Thus, the provided results can be used to prepare for nuclear accidents and improve radiation safety measurements for such incidents.

Author Contributions: Conceptualization, H.M.; methodology, M.Y. and H.M.; software, M.Y.; validation, A.N. and H.M.; formal analysis, M.Y. and R.D.; investigation, M.Y. and R.D.; resources, H.M.; data curation, M.Y. and R.D.; writing—original draft preparation, M.Y.; writing—review and editing, R.D., A.N. and H.M.; visualization, M.Y. and A.N.; supervision, H.M. All authors have read and agreed to the published version of the manuscript.

Funding: This research received no external funding.

Institutional Review Board Statement: Not applicable.

Informed Consent Statement: Not applicable.

Data Availability Statement: Any data request should be directed to the corresponding author, Hanna Moussa (hanna.moussa@ttu.edu).

Conflicts of Interest: The authors declare no conflicts of interest.

Appendix A

Table A1. Skin absorbed dose coefficient values for different energy sources.

Cell Height (cm)	SADC 0.1 MeV (Total)	SADC 0.1 MeV (Electron Only)	SADC 0.2 MeV (Total)	SADC 0.2 MeV (Electron Only)
8	6.27556×10^{-12}	6.04969×10^{-12}	5.17971×10^{-8}	5.17873×10^{-8}
10	3.49948×10^{-13}	2.5631×10^{-13}	4.97467×10^{-8}	4.97367×10^{-8}
12	1.48091×10^{-13}	7.54308×10^{-14}	3.98042×10^{-8}	3.97957×10^{-8}
14	1.15671×10^{-13}	5.76044×10^{-14}	3.09343×10^{-8}	3.09269×10^{-8}
16	7.94832×10^{-14}	3.80907×10^{-14}	2.34543×10^{-8}	2.34479×10^{-8}
18	5.82612×10^{-14}	2.89362×10^{-14}	1.72147×10^{-8}	1.72092×10^{-8}
20	4.38622×10^{-14}	2.1619×10^{-14}	1.18875×10^{-8}	1.18829×10^{-8}
22	3.29422×10^{-14}	1.67262×10^{-14}	7.76607×10^{-9}	7.76232×10^{-9}
24	3.03609×10^{-14}	1.53336×10^{-14}	4.68356×10^{-9}	4.68057×10^{-9}
26	2.12978×10^{-14}	1.12308×10^{-14}	2.57619×10^{-9}	2.57389×10^{-9}
28	1.54008×10^{-14}	8.12283×10^{-15}	1.253×10^{-9}	1.25135×10^{-9}
30	1.6672×10^{-14}	7.81634×10^{-15}	5.30977×10^{-10}	5.29859×10^{-10}
32	1.06824×10^{-14}	5.31659×10^{-15}	1.92356×10^{-10}	1.91631×10^{-10}
34	1.01953×10^{-14}	5.12833×10^{-15}	5.52993×10^{-11}	5.48955×10^{-11}
36	7.93504×10^{-15}	4.02001×10^{-15}	1.42506×10^{-11}	1.40187×10^{-11}
38	8.1733×10^{-15}	3.82112×10^{-15}	3.47246×10^{-12}	3.3317×10^{-12}
40	6.57543×10^{-15}	3.33496×10^{-15}	1.26596×10^{-12}	1.12702×10^{-12}
42	5.43535×10^{-15}	2.79618×10^{-15}	7.73613×10^{-13}	5.67011×10^{-13}
44	3.99769×10^{-15}	2.504×10^{-15}	6.33219×10^{-13}	3.62858×10^{-13}
46	2.19007×10^{-15}	1.11618×10^{-15}	6.07855×10^{-13}	3.11515×10^{-13}
48	2.88994×10^{-15}	1.33791×10^{-15}	5.65247×10^{-13}	2.82757×10^{-13}
50	3.3146×10^{-15}	1.78671×10^{-15}	4.05524×10^{-13}	2.05199×10^{-13}
52	2.5046×10^{-15}	1.38472×10^{-15}	4.80034×10^{-13}	2.39384×10^{-13}
54	2.79076×10^{-15}	1.41675×10^{-15}	4.64174×10^{-13}	2.32038×10^{-13}
56	2.85994×10^{-15}	1.4356×10^{-15}	3.54047×10^{-13}	1.68791×10^{-13}
58	1.74978×10^{-15}	7.73286×10^{-16}	2.55205×10^{-13}	1.2679×10^{-13}

Table A1. *Cont.*

Cell Height (cm)	SADC 0.1 MeV (Total)	SADC 0.1 MeV (Electron Only)	SADC 0.2 MeV (Total)	SADC 0.2 MeV (Electron Only)
60	2.64676×10^{-15}	1.25784×10^{-15}	3.05163×10^{-13}	1.5015×10^{-13}
62	1.42919×10^{-15}	5.28574×10^{-16}	2.76536×10^{-13}	1.41442×10^{-13}
64	7.34606×10^{-16}	3.89442×10^{-16}	2.35564×10^{-13}	1.16183×10^{-13}
66	9.52596×10^{-16}	5.24889×10^{-16}	2.88768×10^{-13}	1.41663×10^{-13}
68	1.03313×10^{-15}	6.14273×10^{-16}	2.09216×10^{-13}	1.06419×10^{-13}
70	1.02064×10^{-15}	5.33462×10^{-16}	3.21689×10^{-13}	1.53746×10^{-13}
72	1.0211×10^{-15}	4.65846×10^{-16}	2.00937×10^{-13}	1.00923×10^{-13}
74	7.93887×10^{-16}	2.31195×10^{-16}	2.01728×10^{-13}	1.04154×10^{-13}
76	1.11199×10^{-15}	6.59262×10^{-16}	1.82569×10^{-13}	9.09997×10^{-14}
78	5.86184×10^{-16}	2.60717×10^{-16}	1.39463×10^{-13}	6.95489×10^{-14}
80	8.80337×10^{-16}	4.21701×10^{-16}	1.78755×10^{-13}	8.73919×10^{-14}
82	7.48739×10^{-16}	3.70453×10^{-16}	1.11334×10^{-13}	5.59451×10^{-14}
84	1.10088×10^{-15}	5.97302×10^{-16}	1.1604×10^{-13}	5.79167×10^{-14}
86	7.67459×10^{-16}	4.3404×10^{-16}	1.46857×10^{-13}	7.44679×10^{-14}
88	4.30537×10^{-16}	1.97844×10^{-16}	1.32768×10^{-13}	6.54113×10^{-14}
90	4.73508×10^{-16}	2.83608×10^{-16}	1.13431×10^{-13}	5.94924×10^{-14}
92	7.37274×10^{-16}	3.98758×10^{-16}	9.47813×10^{-14}	4.70627×10^{-14}
94	2.18959×10^{-16}	4.14658×10^{-17}	7.08436×10^{-14}	3.51179×10^{-14}
96	2.1946×10^{-16}	1.23618×10^{-16}	6.3413×10^{-14}	3.08134×10^{-14}
98	3.8332×10^{-16}	1.51884×10^{-16}	1.05418×10^{-13}	5.54133×10^{-14}
100	4.95157×10^{-16}	1.17279×10^{-16}	7.97614×10^{-14}	3.86298×10^{-14}
102	3.49371×10^{-16}	2.04285×10^{-16}	8.14804×10^{-14}	4.13479×10^{-14}
104	3.22285×10^{-16}	6.69031×10^{-17}	6.17878×10^{-14}	3.32707×10^{-14}
106	2.82602×10^{-16}	1.70301×10^{-16}	8.42694×10^{-14}	4.23136×10^{-14}

SADC 0.4 MeV (Total)	SADC 0.4 MeV (Electron Only)	SADC 0.8 MeV (Total)	SADC 0.8 MeV (Electron Only)	SADC 1.0 MeV (Total)	SADC 1.0 MeV (Electron Only)
3.14306×10^{-8}	3.14236×10^{-8}	3.71331×10^{-8}	3.71206×10^{-8}	3.87557×10^{-8}	3.87402×10^{-8}
3.35304×10^{-8}	3.35219×10^{-8}	3.98432×10^{-8}	3.98315×10^{-8}	4.13645×10^{-8}	4.13495×10^{-8}
3.15434×10^{-8}	3.15365×10^{-8}	3.86493×10^{-8}	3.86363×10^{-8}	4.02664×10^{-8}	4.02502×10^{-8}
2.97547×10^{-8}	2.97475×10^{-8}	3.73593×10^{-8}	3.7347×10^{-8}	3.88599×10^{-8}	3.88451×10^{-8}
2.79693×10^{-8}	2.79623×10^{-8}	3.62962×10^{-8}	3.6283×10^{-8}	3.82832×10^{-8}	3.82679×10^{-8}
2.63882×10^{-8}	2.63822×10^{-8}	3.49538×10^{-8}	3.4942×10^{-8}	3.66882×10^{-8}	3.66742×10^{-8}
2.49211×10^{-8}	2.49149×10^{-8}	3.40601×10^{-8}	3.4049×10^{-8}	3.60246×10^{-8}	3.60108×10^{-8}
2.34914×10^{-8}	2.34861×10^{-8}	3.2964×10^{-8}	3.2953×10^{-8}	3.49379×10^{-8}	3.49242×10^{-8}
2.2119×10^{-8}	2.40647×10^{-8}	3.21937×10^{-8}	3.2183×10^{-8}	3.44987×10^{-8}	3.44853×10^{-8}
2.08857×10^{-8}	2.08806×10^{-8}	3.14558×10^{-8}	3.14448×10^{-8}	3.37317×10^{-8}	3.37177×10^{-8}
1.96906×10^{-8}	1.96857×10^{-8}	3.0552×10^{-8}	3.05417×10^{-8}	3.25048×10^{-8}	3.24921×10^{-8}
1.85601×10^{-8}	1.85561×10^{-8}	2.95743×10^{-8}	2.95642×10^{-8}	3.1991×10^{-8}	3.19789×10^{-8}
1.74731×10^{-8}	1.7469×10^{-8}	2.89703×10^{-8}	2.89606×10^{-8}	3.19365×10^{-8}	3.1924×10^{-8}

Table A1. *Cont.*

SADC 0.4 MeV (Total)	SADC 0.4 MeV (Electron Only)	SADC 0.8 MeV (Total)	SADC 0.8 MeV (Electron Only)	SADC 1.0 MeV (Total)	SADC 1.0 MeV (Electron Only)
1.65135×10^{-8}	1.65095×10^{-8}	2.84946×10^{-8}	2.84851×10^{-8}	3.07177×10^{-8}	3.07057×10^{-8}
1.5453×10^{-8}	1.54487×10^{-8}	2.75534×10^{-8}	2.75434×10^{-8}	3.00535×10^{-8}	3.00419×10^{-8}
1.461×10^{-8}	1.46061×10^{-8}	2.68904×10^{-8}	2.68806×10^{-8}	2.93964×10^{-8}	2.93847×10^{-8}
1.36546×10^{-8}	1.36511×10^{-8}	2.62921×10^{-8}	2.62825×10^{-8}	2.89998×10^{-8}	2.89882×10^{-8}
1.26872×10^{-8}	1.26832×10^{-8}	2.58724×10^{-8}	2.58633×10^{-8}	2.81526×10^{-8}	2.81412×10^{-8}
1.18984×10^{-8}	1.18952×10^{-8}	2.53118×10^{-8}	2.53028×10^{-8}	2.78858×10^{-8}	2.78741×10^{-8}
1.10589×10^{-8}	1.10561×10^{-8}	2.44213×10^{-8}	2.44132×10^{-8}	2.76×10^{-8}	2.75892×10^{-8}
1.02906×10^{-8}	1.02877×10^{-8}	2.3911×10^{-8}	2.39023×10^{-8}	2.71368×10^{-8}	2.71264×10^{-8}
9.50825×10^{-9}	9.50546×10^{-9}	2.35808×10^{-8}	2.35723×10^{-8}	2.61447×10^{-8}	2.61337×10^{-8}
8.75714×10^{-9}	8.75464×10^{-9}	2.28001×10^{-8}	2.27923×10^{-8}	2.59255×10^{-8}	2.59152×10^{-8}
8.06402×10^{-9}	8.06152×10^{-9}	2.24159×10^{-8}	2.24083×10^{-8}	2.53628×10^{-8}	2.53527×10^{-8}
7.37938×10^{-9}	7.37738×10^{-9}	2.19578×10^{-8}	2.195×10^{-8}	2.50483×10^{-8}	2.50381×10^{-8}
6.7417×10^{-9}	6.73961×10^{-9}	2.13707×10^{-8}	2.13629×10^{-8}	2.42554×10^{-8}	2.42455×10^{-8}
6.06397×10^{-9}	6.06218×10^{-9}	2.10356×10^{-8}	2.10278×10^{-8}	2.44312×10^{-8}	2.4421×10^{-8}
5.4638×10^{-9}	6.62567×10^{-9}	2.05911×10^{-8}	2.05836×10^{-8}	2.35574×10^{-8}	2.35477×10^{-8}
4.8893×10^{-9}	4.88762×10^{-9}	2.00101×10^{-8}	2.0003×10^{-8}	2.31366×10^{-8}	2.31273×10^{-8}
4.37482×10^{-9}	4.37343×10^{-9}	1.95563×10^{-8}	1.95495×10^{-8}	2.29404×10^{-8}	2.29308×10^{-8}
3.83669×10^{-9}	3.8354×10^{-9}	1.92875×10^{-8}	1.92804×10^{-8}	2.26207×10^{-8}	2.26112×10^{-8}
3.3598×10^{-9}	3.35854×10^{-9}	1.88643×10^{-8}	1.88577×10^{-8}	2.2127×10^{-8}	2.21175×10^{-8}
2.92522×10^{-9}	2.90008×10^{-9}	1.83822×10^{-8}	1.83754×10^{-8}	2.19156×10^{-8}	2.19063×10^{-8}
2.49481×10^{-9}	2.48722×10^{-9}	1.79079×10^{-8}	1.79012×10^{-8}	2.16257×10^{-8}	2.16162×10^{-8}
2.13793×10^{-9}	2.12477×10^{-9}	1.75758×10^{-8}	1.75693×10^{-8}	2.13088×10^{-8}	2.12997×10^{-8}
1.80001×10^{-9}	1.77208×10^{-9}	1.73691×10^{-8}	1.73626×10^{-8}	2.05987×10^{-8}	2.05897×10^{-8}
1.49755×10^{-9}	1.5238×10^{-9}	1.69167×10^{-8}	1.69104×10^{-8}	2.03303×10^{-8}	2.03218×10^{-8}
1.23233×10^{-9}	1.24209×10^{-9}	1.65557×10^{-8}	1.65498×10^{-8}	2.00776×10^{-8}	2.00692×10^{-8}
1.00011×10^{-9}	9.91292×10^{-10}	1.62468×10^{-8}	1.62404×10^{-8}	1.97985×10^{-8}	1.97902×10^{-8}
8.01972×10^{-10}	8.18378×10^{-10}	1.58755×10^{-8}	1.58696×10^{-8}	1.93064×10^{-8}	1.9298×10^{-8}
6.26823×10^{-10}	6.30403×10^{-10}	1.54783×10^{-8}	1.54723×10^{-8}	1.92712×10^{-8}	1.92627×10^{-8}
4.83981×10^{-10}	4.82477×10^{-10}	1.52549×10^{-8}	1.52493×10^{-8}	1.88957×10^{-8}	1.88879×10^{-8}
3.66043×10^{-10}	3.83834×10^{-10}	1.49319×10^{-8}	1.49263×10^{-8}	1.862×10^{-8}	1.86122×10^{-8}
2.75858×10^{-10}	2.6864×10^{-10}	1.46126×10^{-8}	1.46071×10^{-8}	1.82247×10^{-8}	1.8217×10^{-8}
1.99562×10^{-10}	1.93692×10^{-10}	1.40584×10^{-8}	1.40531×10^{-8}	1.79156×10^{-8}	1.79077×10^{-8}
1.38245×10^{-10}	1.2183×10^{-10}	1.39193×10^{-8}	1.39139×10^{-8}	1.76165×10^{-8}	1.76088×10^{-8}
9.95857×10^{-11}	1.04006×10^{-10}	1.36202×10^{-8}	1.3615×10^{-8}	1.75089×10^{-8}	1.75014×10^{-8}
6.3325×10^{-11}	7.51687×10^{-11}	1.31612×10^{-8}	1.3156×10^{-8}	1.72524×10^{-8}	1.72449×10^{-8}
4.36845×10^{-11}	4.576×10^{-11}	1.3083×10^{-8}	1.3078×10^{-8}	1.69807×10^{-8}	1.69733×10^{-8}
2.60868×10^{-11}	2.57599×10^{-11}	1.28412×10^{-8}	1.28362×10^{-8}	1.68421×10^{-8}	1.68348×10^{-8}

Table A1. *Cont.*

SADC 1.5 MeV (Total)	SADC 1.5 MeV (Electron Only)	SADC 2.0 MeV (Total)	SADC 2.0 MeV (Electron Only)	SADC 2.5 MeV (Total)	SADC 2.5 MeV (Electron Only)
4.02822×10^{-8}	4.02612×10^{-8}	4.22774×10^{-8}	4.22438×10^{-8}	4.28428×10^{-8}	4.2798×10^{-8}
4.35781×10^{-8}	4.35533×10^{-8}	4.46211×10^{-8}	4.45885×10^{-8}	4.39318×10^{-8}	4.38886×10^{-8}
4.20559×10^{-8}	4.20323×10^{-8}	4.42184×10^{-8}	4.41868×10^{-8}	4.47688×10^{-8}	4.47216×10^{-8}
4.16521×10^{-8}	4.16298×10^{-8}	4.23838×10^{-8}	4.23528×10^{-8}	4.31496×10^{-8}	4.31075×10^{-8}
4.04743×10^{-8}	4.04523×10^{-8}	4.27443×10^{-8}	4.27131×10^{-8}	4.27223×10^{-8}	4.26751×10^{-8}
4.0158×10^{-8}	4.01361×10^{-8}	3.98282×10^{-8}	3.97955×10^{-8}	3.97683×10^{-8}	3.97307×10^{-8}
3.91374×10^{-8}	3.91137×10^{-8}	4.00275×10^{-8}	3.99957×10^{-8}	4.02321×10^{-8}	4.01864×10^{-8}
3.786×10^{-8}	3.78401×10^{-8}	3.94357×10^{-8}	3.9405×10^{-8}	4.0393×10^{-8}	4.03481×10^{-8}
3.76174×10^{-8}	3.75969×10^{-8}	3.89091×10^{-8}	3.88786×10^{-8}	3.87127×10^{-8}	3.8673×10^{-8}
3.69208×10^{-8}	3.69009×10^{-8}	3.72031×10^{-8}	3.71758×10^{-8}	3.85987×10^{-8}	3.85558×10^{-8}
3.58793×10^{-8}	3.58614×10^{-8}	3.76659×10^{-8}	3.76393×10^{-8}	3.94718×10^{-8}	3.9432×10^{-8}
3.55385×10^{-8}	3.55182×10^{-8}	3.72394×10^{-8}	3.72079×10^{-8}	3.71736×10^{-8}	3.71339×10^{-8}
3.45592×10^{-8}	3.45396×10^{-8}	3.57131×10^{-8}	3.5686×10^{-8}	3.75834×10^{-8}	3.75445×10^{-8}
3.37135×10^{-8}	3.3695×10^{-8}	3.54866×10^{-8}	3.5458×10^{-8}	3.58372×10^{-8}	3.57988×10^{-8}
3.36703×10^{-8}	3.36508×10^{-8}	3.53362×10^{-8}	3.53083×10^{-8}	3.71197×10^{-8}	3.70825×10^{-8}
3.34957×10^{-8}	3.34771×10^{-8}	3.43453×10^{-8}	3.43203×10^{-8}	3.57416×10^{-8}	3.57036×10^{-8}
3.2392×10^{-8}	3.23734×10^{-8}	3.4965×10^{-8}	3.49368×10^{-8}	3.53907×10^{-8}	3.51735×10^{-8}
3.1969×10^{-8}	3.19518×10^{-8}	3.37118×10^{-8}	3.36833×10^{-8}	3.44374×10^{-8}	3.4398×10^{-8}
3.1301×10^{-8}	3.12826×10^{-8}	3.35855×10^{-8}	3.356×10^{-8}	3.4374×10^{-8}	3.43377×10^{-8}
3.12536×10^{-8}	3.12355×10^{-8}	3.35501×10^{-8}	3.35249×10^{-8}	3.38086×10^{-8}	3.37751×10^{-8}
3.06733×10^{-8}	3.06543×10^{-8}	3.27337×10^{-8}	3.2707×10^{-8}	3.31598×10^{-8}	3.31261×10^{-8}
3.02872×10^{-8}	3.02702×10^{-8}	3.27121×10^{-8}	3.26868×10^{-8}	3.34841×10^{-8}	3.34462×10^{-8}
2.96346×10^{-8}	2.96192×10^{-8}	3.20571×10^{-8}	3.20331×10^{-8}	3.29261×10^{-8}	3.28933×10^{-8}
2.90777×10^{-8}	2.90615×10^{-8}	3.14669×10^{-8}	3.14416×10^{-8}	3.2582×10^{-8}	3.25497×10^{-8}
2.91561×10^{-8}	2.91385×10^{-8}	3.08501×10^{-8}	3.08261×10^{-8}	3.24511×10^{-8}	3.2419×10^{-8}
2.84802×10^{-8}	2.84642×10^{-8}	3.18758×10^{-8}	3.18523×10^{-8}	3.18086×10^{-8}	3.1778×10^{-8}
2.89623×10^{-8}	2.89453×10^{-8}	3.05075×10^{-8}	3.04845×10^{-8}	3.17572×10^{-8}	3.17235×10^{-8}
2.85121×10^{-8}	2.84956×10^{-8}	2.95877×10^{-8}	2.95623×10^{-8}	3.16766×10^{-8}	3.16454×10^{-8}
2.79915×10^{-8}	2.79752×10^{-8}	2.92609×10^{-8}	2.92387×10^{-8}	3.01892×10^{-8}	2.94404×10^{-8}
2.72598×10^{-8}	2.7244×10^{-8}	2.97286×10^{-8}	2.97057×10^{-8}	2.97902×10^{-8}	2.97587×10^{-8}
2.75966×10^{-8}	2.75811×10^{-8}	2.96975×10^{-8}	2.96749×10^{-8}	3.02458×10^{-8}	3.02159×10^{-8}
2.70389×10^{-8}	2.70235×10^{-8}	2.92857×10^{-8}	2.92619×10^{-8}	2.97321×10^{-8}	2.9697×10^{-8}
2.61642×10^{-8}	2.61485×10^{-8}	2.89833×10^{-8}	2.89606×10^{-8}	2.92305×10^{-8}	2.9199×10^{-8}
2.58267×10^{-8}	2.58111×10^{-8}	2.83458×10^{-8}	2.83223×10^{-8}	2.99053×10^{-8}	2.98729×10^{-8}
2.56272×10^{-8}	2.56117×10^{-8}	2.79668×10^{-8}	2.79438×10^{-8}	2.91888×10^{-8}	2.9159×10^{-8}
2.58161×10^{-8}	2.5801×10^{-8}	2.81231×10^{-8}	2.80993×10^{-8}	2.80607×10^{-8}	2.80304×10^{-8}
2.53749×10^{-8}	2.53607×10^{-8}	2.80203×10^{-8}	2.79989×10^{-8}	2.98294×10^{-8}	2.97998×10^{-8}
2.49378×10^{-8}	2.4923×10^{-8}	2.77227×10^{-8}	2.76993×10^{-8}	2.92661×10^{-8}	2.92378×10^{-8}

Table A1. *Cont.*

SADC 1.5 MeV (Total)	SADC 1.5 MeV (Electron Only)	SADC 2.0 MeV (Total)	SADC 2.0 MeV (Electron Only)	SADC 2.5 MeV (Total)	SADC 2.5 MeV (Electron Only)
2.49891×10^{-8}	2.49737×10^{-8}	2.72965×10^{-8}	2.72749×10^{-8}	2.81004×10^{-8}	2.8071×10^{-8}
2.46617×10^{-8}	2.46473×10^{-8}	2.72949×10^{-8}	2.72716×10^{-8}	2.7669×10^{-8}	2.76403×10^{-8}
2.42575×10^{-8}	2.42437×10^{-8}	2.63802×10^{-8}	2.6361×10^{-8}	2.83591×10^{-8}	2.83309×10^{-8}
2.3826×10^{-8}	2.38118×10^{-8}	2.67228×10^{-8}	2.67015×10^{-8}	2.79499×10^{-8}	2.79198×10^{-8}
2.35034×10^{-8}	2.34895×10^{-8}	2.58826×10^{-8}	2.58609×10^{-8}	2.72681×10^{-8}	2.72404×10^{-8}
2.37087×10^{-8}	2.36953×10^{-8}	2.67065×10^{-8}	2.66863×10^{-8}	2.72896×10^{-8}	2.72609×10^{-8}
2.34147×10^{-8}	2.33999×10^{-8}	2.63057×10^{-8}	2.62846×10^{-8}	2.73034×10^{-8}	2.72769×10^{-8}
2.33797×10^{-8}	2.3367×10^{-8}	2.54557×10^{-8}	2.54354×10^{-8}	2.7489×10^{-8}	2.7459×10^{-8}
2.26179×10^{-8}	2.26052×10^{-8}	2.55735×10^{-8}	2.55528×10^{-8}	2.63682×10^{-8}	2.6339×10^{-8}
2.27819×10^{-8}	2.27676×10^{-8}	2.53802×10^{-8}	2.53602×10^{-8}	2.65219×10^{-8}	2.64937×10^{-8}
2.24591×10^{-8}	2.24455×10^{-8}	2.52146×10^{-8}	2.51934×10^{-8}	2.6675×10^{-8}	2.66459×10^{-8}
2.20536×10^{-8}	2.16054×10^{-8}	2.47716×10^{-8}	2.47535×10^{-8}	2.66325×10^{-8}	2.66055×10^{-8}

SADC 3.0 MeV (Total)	SADC 3.0 MeV (Electron Only)	SADC 4.0 MeV (Total)	SADC 4.0 MeV (Electron Only)
4.20511×10^{-8}	4.1998×10^{-8}	4.58802×10^{-8}	4.57834×10^{-8}
4.45277×10^{-8}	4.4472×10^{-8}	4.69229×10^{-8}	4.68391×10^{-8}
4.45175×10^{-8}	4.4463×10^{-8}	4.75976×10^{-8}	4.75095×10^{-8}
4.23205×10^{-8}	4.22706×10^{-8}	4.53908×10^{-8}	4.46769×10^{-8}
4.32902×10^{-8}	4.32353×10^{-8}	4.3412×10^{-8}	4.33252×10^{-8}
4.05345×10^{-8}	4.04797×10^{-8}	4.28062×10^{-8}	4.27183×10^{-8}
4.13216×10^{-8}	4.1269×10^{-8}	4.42347×10^{-8}	4.41496×10^{-8}
4.05335×10^{-8}	4.04834×10^{-8}	4.47187×10^{-8}	4.46321×10^{-8}
3.96911×10^{-8}	3.96404×10^{-8}	4.25847×10^{-8}	4.4726×10^{-8}
4.04927×10^{-8}	4.04379×10^{-8}	4.12922×10^{-8}	4.12035×10^{-8}
4.03101×10^{-8}	4.02574×10^{-8}	3.986×10^{-8}	3.97829×10^{-8}
3.96804×10^{-8}	3.96315×10^{-8}	4.12521×10^{-8}	4.11665×10^{-8}
3.7577×10^{-8}	3.75301×10^{-8}	3.99838×10^{-8}	3.99013×10^{-8}
3.74613×10^{-8}	3.7418×10^{-8}	3.88705×10^{-8}	3.87953×10^{-8}
3.64923×10^{-8}	3.64333×10^{-8}	3.86586×10^{-8}	3.85915×10^{-8}
3.57357×10^{-8}	3.56946×10^{-8}	3.853×10^{-8}	3.84546×10^{-8}
3.5634×10^{-8}	3.55886×10^{-8}	3.85997×10^{-8}	3.85212×10^{-8}
3.47664×10^{-8}	3.47146×10^{-8}	3.70396×10^{-8}	3.69637×10^{-8}
3.46103×10^{-8}	3.45674×10^{-8}	3.78387×10^{-8}	3.77595×10^{-8}
3.44836×10^{-8}	3.4439×10^{-8}	3.5778×10^{-8}	3.57084×10^{-8}
3.41062×10^{-8}	3.37894×10^{-8}	3.58706×10^{-8}	3.58017×10^{-8}
3.32799×10^{-8}	3.32387×10^{-8}	3.69322×10^{-8}	3.6855×10^{-8}
3.38445×10^{-8}	3.38002×10^{-8}	3.42048×10^{-8}	3.41373×10^{-8}

Table A1. *Cont.*

SADC 3.0 MeV (Total)	SADC 3.0 MeV (Electron Only)	SADC 4.0 MeV (Total)	SADC 4.0 MeV (Electron Only)
3.36898×10^{-8}	3.36469×10^{-8}	3.56404×10^{-8}	3.55644×10^{-8}
3.44036×10^{-8}	3.43601×10^{-8}	3.28853×10^{-8}	3.282×10^{-8}
3.27176×10^{-8}	3.26751×10^{-8}	3.61148×10^{-8}	3.60441×10^{-8}
3.21002×10^{-8}	3.20555×10^{-8}	3.33296×10^{-8}	3.32635×10^{-8}
3.21583×10^{-8}	3.21148×10^{-8}	3.3475×10^{-8}	3.34041×10^{-8}
3.16253×10^{-8}	3.12094×10^{-8}	3.46265×10^{-8}	3.45599×10^{-8}
3.10999×10^{-8}	3.1059×10^{-8}	3.35655×10^{-8}	3.34982×10^{-8}
3.12104×10^{-8}	3.11717×10^{-8}	3.46085×10^{-8}	3.45394×10^{-8}
3.05309×10^{-8}	3.04933×10^{-8}	3.19524×10^{-8}	3.18923×10^{-8}
3.12222×10^{-8}	3.11797×10^{-8}	3.33362×10^{-8}	3.3277×10^{-8}
3.03118×10^{-8}	2.92382×10^{-8}	3.22444×10^{-8}	3.21825×10^{-8}
2.95433×10^{-8}	2.95025×10^{-8}	3.30793×10^{-8}	3.3009×10^{-8}
3.05812×10^{-8}	3.05413×10^{-8}	3.11085×10^{-8}	3.10506×10^{-8}
3.01425×10^{-8}	3.01027×10^{-8}	3.1875×10^{-8}	3.1818×10^{-8}
2.83938×10^{-8}	2.83573×10^{-8}	3.03722×10^{-8}	3.02523×10^{-8}
3.04715×10^{-8}	3.04315×10^{-8}	3.3109×10^{-8}	3.30421×10^{-8}
2.98686×10^{-8}	2.98263×10^{-8}	3.2297×10^{-8}	3.22284×10^{-8}
2.89078×10^{-8}	2.88681×10^{-8}	3.04955×10^{-8}	3.04358×10^{-8}
2.87648×10^{-8}	2.87283×10^{-8}	3.0208×10^{-8}	3.01498×10^{-8}
2.95522×10^{-8}	2.86641×10^{-8}	3.02883×10^{-8}	3.02293×10^{-8}
2.80486×10^{-8}	2.80137×10^{-8}	3.02007×10^{-8}	3.01423×10^{-8}
2.82728×10^{-8}	2.82342×10^{-8}	3.09922×10^{-8}	3.09288×10^{-8}
2.7294×10^{-8}	2.72597×10^{-8}	3.14406×10^{-8}	3.13808×10^{-8}
2.74851×10^{-8}	2.74505×10^{-8}	2.9558×10^{-8}	2.95043×10^{-8}
2.74629×10^{-8}	2.74276×10^{-8}	2.87861×10^{-8}	2.87294×10^{-8}
2.62886×10^{-8}	2.6256×10^{-8}	2.96314×10^{-8}	2.95688×10^{-8}
2.75767×10^{-8}	2.75428×10^{-8}	2.91121×10^{-8}	2.90592×10^{-8}

References

1. Rojavin, Y.; Seamon, M.J.; Tripathi, R.S.; Papadimos, T.J.; Galwankar, S.; Kman, N.; Cipolla, J.; Grossman, M.D.; Marchigiani, R.; Stawicki, S.P. Civilian nuclear incidents: An overview of historical, medical, and scientific aspects. *J. Emergencies Trauma Shock* **2011**, *4*, 260.
2. Dent, R.A. Management of Casualties from Radiation Events. *Eur. Burn J.* **2023**, *4*, 584–595. [CrossRef]
3. Molé, D.M. Introduction to nuclear and radiological disasters. In *Ciottone's Disaster Medicine*; Elsevier: Amsterdam, The Netherlands, 2024; pp. 647–652.
4. Hatch, M.; Ron, E.; Bouville, A.; Zablotska, L.; Howe, G. The Chernobyl disaster: Cancer following the accident at the Chernobyl nuclear power plant. *Epidemiol. Rev.* **2005**, *27*, 56–66. [CrossRef]
5. Luckey, T.D. *Radiation Hormesis*; CRC Press: Boca Raton, FL, USA, 2020.
6. Barabanova, A.V. Significance of beta-radiation skin burns in Chernobyl patients for the theory and practice of radiopathology. *Vojnosanit. Pregl.* **2006**, *63*, 477–480. [CrossRef] [PubMed]
7. Yamamoto, S.; Ishibashi, H. Development of a three-layer phoswich alpha–beta–gamma imaging detector. *Nucl. Instrum. Methods Phys. Res. Sect. A Accel. Spectrometers Detect. Assoc. Equip.* **2015**, *785*, 129–134. [CrossRef]
8. Obrador, E.; Salvador-Palmer, R.; Villaescusa, J.I.; Gallego, E.; Pellicer, B.; Estrela, J.M.; Montoro, A. Nuclear and radiological emergencies: Biological effects, countermeasures and biodosimetry. *Antioxidants* **2022**, *11*, 1098. [CrossRef]

9. L'annunziata, M.F. *Radioactivity: Introduction and History, from the Quantum to Quarks*; Elsevier: Amsterdam, The Netherlands, 2016.
10. L'Annunziata, M.F. *Handbook of Radioactivity Analysis*; Academic Press: Cambridge, MA, USA, 2012.
11. L'Annunziata, M. Gamma-and X-Radiation—Photons. In *Radioactivity: Introduction and History*, 1st ed.; Elsevier: Amsterdam, The Netherlands, 2007; pp. 187–215.
12. Airey, P.; Hinton, T.; Twining, J. The Scientific Basis. In *Radioactivity in the Environment*; Elsevier: Amsterdam, The Netherlands, 2012; Volume 18, pp. 1–57.
13. Vergados, J.; Ejiri, H.; Šimkovic, F. Theory of neutrinoless double-beta decay. *Rep. Prog. Phys.* **2012**, *75*, 106301. [CrossRef]
14. Jenkins, D. *Radiation Detection for Nuclear Physics*; IOP Publishing: Bristol, UK, 2020.
15. Iddins, C.J.; DiCarlo, A.L.; Ervin, M.D.; Herrera-Reyes, E.; Goans, R.E. Cutaneous and local radiation injuries. *J. Radiol. Prot.* **2022**, *42*, 011001. [CrossRef]
16. Talapko, J.; Talapko, D.; Katalinić, D.; Kotris, I.; Erić, I.; Belić, D.; Vasilj Mihaljević, M.; Vasilj, A.; Erić, S.; Flam, J. Health Effects of Ionizing Radiation on the Human Body. *Medicina* **2024**, *60*, 653. [CrossRef]
17. Ghazwani, M.; Hani, U.; Alqarni, M.H.; Alam, A. Beta caryophyllene-loaded nanostructured lipid carriers for topical management of skin disorders: Statistical optimization, in vitro and dermatokinetic evaluation. *Gels* **2023**, *9*, 550. [CrossRef]
18. Fujisawa, M.; Haga, Y.; Sota, M.; Abe, M.; Kaga, Y.; Inaba, Y.; Suzuki, M.; Meguro, T.; Hosoi, Y.; Chida, K. Evaluation of lens doses among medical staff involved in nuclear medicine: Current eye radiation exposure among nuclear-medicine staff. *Appl. Sci.* **2023**, *13*, 9182. [CrossRef]
19. Tanzifi, G.; Koshki, A.A. Translation of Radiation Protection in Nuclear Medicine. *Eurasian J. Chem. Med. Pet. Res.* **2024**, *3*, 775–781.
20. Eckerman, K.; Endo, A. ICRP Publication 107. Nuclear decay data for dosimetric calculations. *Ann. ICRP* **2008**, *38*, 7–96. [PubMed]
21. Kang, H.; Min, S.; Seo, B.; Roh, C.; Hong, S.; Cheong, J.H. Low energy beta emitter measurement: A review. *Chemosensors* **2020**, *8*, 106. [CrossRef]
22. Cross, W.; Ing, H.; Freedman, N. A short atlas of beta-ray spectra. *Phys. Med. Biol.* **1983**, *28*, 1251. [CrossRef]
23. Hsu, H.-H.; Chen, J.; Ing, H.; Clifford, E.; McLean, T. Skin dose measurement with microspec-2TM. *Nucl. Instrum. Methods Phys. Res. Sect. A Accel. Spectrometers Detect. Assoc. Equip.* **1998**, *412*, 155–160. [CrossRef]
24. Faw, R.E. Absorbed doses to skin from radionuclide sources on the body surface. *Health Phys.* **1992**, *63*, 443–448. [CrossRef]
25. Hamby, D.M.; Mangini, C.D.; Caffrey, J.A.; Tang, M. *VARSKIN 5: A Computer Code for Skin Contamination Dosimetry*; United States Nuclear Regulatory Commission, Office of Nuclear Regulatory: Rockville, MD, USA, 2014.
26. Sherbini, S.; DeCicco, J.; Gray, A.T.; Struckmeyer, R. Verification of the VARSKIN beta skin dose calculation computer code. *Health Phys.* **2008**, *94*, 527–538. [CrossRef]
27. Amato, E.; Italiano, A. Evaluation of skin absorbed doses during manipulation of radioactive sources: A comparison between the VARSKIN code and Monte Carlo simulations. *J. Radiol. Prot.* **2018**, *38*, 262. [CrossRef] [PubMed]
28. Misdaq, M.; Harrass, H.; Saikouk, H.; Matrane, A. Dose to Medical Personnel. *Health Phys.* **2020**, *118*, 129–135. [CrossRef]
29. Agostinelli, S.; Allison, J.; Amako, K.a.; Apostolakis, J.; Araujo, H.; Arce, P.; Asai, M.; Axen, D.; Banerjee, S.; Barrand, G. GEANT4—A simulation toolkit. *Nucl. Instrum. Methods Phys. Res. Sect. A Accel. Spectrometers Detect. Assoc. Equip.* **2003**, *506*, 250–303. [CrossRef]
30. Kotroumpelou, C.; Kyriakou, I.; Ivanchenko, V.; Incerti, S.; Emfietzoglou, D. Electron Absorbed Fractions and S Factors for Intermediate Size Target Volumes: Comparison of Analytic Calculations and Monte Carlo Simulations. *Appl. Sci.* **2024**, *14*, 2275. [CrossRef]
31. Chow, J.C.; Santiago, C.A. DNA damage of iron-gold nanoparticle heterojunction irradiated by kV photon beams: A monte carlo study. *Appl. Sci.* **2023**, *13*, 8942. [CrossRef]
32. Kadri, O.; Alfuraih, A. Buildup Factor Computation and Percentage Depth Dose Simulation of Tissue Mimicking Materials for an External Photon Beam (0.15–15 MeV). *Appl. Sci.* **2022**, *12*, 4250. [CrossRef]
33. Frosio, T.; Bertreix, P.; Menaa, N.; Thomas, S. Calculation and benchmark of fluence-to-local skin equivalent dose coefficients for neutrons with FLUKA, MCNP, and GEANT4 Monte-Carlo codes. *J. Radiol. Prot.* **2021**, *41*, 564. [CrossRef] [PubMed]
34. Berger, M.J. Improved point kernels for electron and beta-ray dosimetry. *Rep. NBSIR* **1973**, *107*, 73–107.
35. Eckerman, K. *External Exposure to Radionuclides in Air, Water, and Soil [Microform]*; Oak Ridge National Laboratory: Oak Ridge, TN, USA, 1993.
36. Bellamy, M.; Dewji, S.; Leggett, R.; Hiller, M.; Veinot, K.; Manger, R.; Eckerman, K.; Ryman, J.; Easterly, C.; Hertel, N. *External Exposure to Radionuclides in Air, Water, and Soil*; Federal Guidance Report NO. 15; Oak Ridge National Laboratory: Oak Ridge, TN, USA, 2019.
37. Arce, P.; Bolst, D.; Bordage, M.C.; Brown, J.; Cirrone, P.; Cortés-Giraldo, M.A.; Cutajar, D.; Cuttone, G.; Desorgher, L.; Dondero, P. Report on G4-Med, a Geant4 benchmarking system for medical physics applications developed by the Geant4 Medical Simulation Benchmarking Group. *Med. Phys.* **2021**, *48*, 19–56. [CrossRef]
38. Dhakal, R.; Yosofvand, M.; Moussa, H. Development and Application of MAGIC-f Gel in Cancer Research and Medical Imaging. *Appl. Sci.* **2021**, *11*, 7783. [CrossRef]
39. Loffredo, F.; Vardaci, E.; Bianco, D.; Di Nitto, A.; Quarto, M. Protons interaction with Nomex target: Secondary Radiation from a Monte Carlo simulation with Geant4. *Appl. Sci.* **2022**, *12*, 2643. [CrossRef]
40. Berger, M.J.; Seltzer, S.M. *Stopping Powers and Ranges of Electrons and Positrons*, 2nd ed.; Center for Radiation Research, National Bureau of Standards: Washington, DC, USA, 1982.

41. Usta, M. Continuous slowing-down approximation ranges of biological materials for 0.05–10 MeV alpha particles by using different approach methods. *Appl. Radiat. Isot.* **2021**, *178*, 109951. [CrossRef]
42. Turner, J.E. *Atoms, Radiation, and Radiation Protection*; John Wiley & Sons: Hoboken, NJ, USA, 2008.
43. Powell, C.J.; Jablonski, A. The NIST electron effective-attenuation-length database. *J. Surf. Anal.* **2002**, *9*, 322–325. [CrossRef]
44. Sjövall, P.; Skedung, L.; Gregoire, S.; Biganska, O.; Clément, F.; Luengo, G.S. Imaging the distribution of skin lipids and topically applied compounds in human skin using mass spectrometry. *Sci. Rep.* **2018**, *8*, 1–14. [CrossRef] [PubMed]
45. de Oliveira, N.F.P.; de Souza, B.F.; de Castro Coêlho, M. Uv radiation and its relation to DNA methylation in epidermal cells: A review. *Epigenomes* **2020**, *4*, 23. [CrossRef]
46. Veltri, A.; Lang, C.; Lien, W.-H. Concise review: Wnt signaling pathways in skin development and epidermal stem cells. *Stem Cells* **2018**, *36*, 22–35. [CrossRef] [PubMed]
47. i Garau, M.M.; Calduch, A.L.; López, E.C. Radiobiology of the acute radiation syndrome. *Rep. Pract. Oncol. Radiother.* **2011**, *16*, 123–130. [CrossRef] [PubMed]
48. White, S.C.; Pharoah, M.J. *Oral radiology-E-Book: Principles and interpretation*; Elsevier Health Sciences: Amsterdam, The Netherlands, 2014.
49. Shih, B.B.; Farrar, M.D.; Cooke, M.S.; Osman, J.; Langton, A.K.; Kift, R.; Webb, A.R.; Berry, J.L.; Watson, R.E.; Vail, A. Fractional sunburn threshold UVR doses generate equivalent vitamin D and DNA damage in skin types I–VI but with epidermal DNA damage gradient correlated to skin darkness. *J. Investig. Dermatol.* **2018**, *138*, 2244–2252. [CrossRef] [PubMed]
50. Watt, T.C.; Inskip, P.D.; Stratton, K.; Smith, S.A.; Kry, S.F.; Sigurdson, A.J.; Stovall, M.; Leisenring, W.; Robison, L.L.; Mertens, A.C. Radiation-related risk of basal cell carcinoma: A report from the Childhood Cancer Survivor Study. *J. Natl. Cancer Inst.* **2012**, *104*, 1240–1250. [CrossRef] [PubMed]
51. Petoussi-Henss, N.; Bolch, W.; Eckerman, K.; Endo, A.; Hertel, N.; Hunt, J.; Pelliccioni, M.; Schlattl, H.; Zankl, M. Conversion coefficients for radiological protection quantities for external radiation exposures. *Ann. ICRP* **2010**, *40*, 1–257. [CrossRef] [PubMed]
52. Hopewell, J. The skin: Its structure and response to ionizing radiation. *Int. J. Radiat. Biol.* **1990**, *57*, 751–773. [CrossRef] [PubMed]
53. Whitton, J.T.; Everall, J. The thickness of the epidermis. *Br. J. Dermatol.* **1973**, *89*, 467–476. [CrossRef]
54. El-Ouardi, Y.; Dadouch, A.; Aknouch, A.; Mouhib, M.; Maghnouj, A.; Didi, A. Comparative Study Between Geant4, MCNP6 and Experimental Results Against Gamma Radiation Comes from a Cobalt-60 Source. *Mosc. Univ. Phys. Bull.* **2020**, *75*, 507–511. [CrossRef]

Disclaimer/Publisher's Note: The statements, opinions and data contained in all publications are solely those of the individual author(s) and contributor(s) and not of MDPI and/or the editor(s). MDPI and/or the editor(s) disclaim responsibility for any injury to people or property resulting from any ideas, methods, instructions or products referred to in the content.